Inbound Carrier Plan Optimization for Adaptive VSAT Networks

CLEMENT LACOSTE
Interdisciplinary Center for Security, Reliability and Trust (SnT), Luxembourg, Luxembourg

WALLACE A. MARTINS, Senior Member, IEEE
Interdisciplinary Center for Security, Reliability and Trust (SnT), Luxembourg, Luxembourg

SYMEON CHATZINOTAS, Senior Member, IEEE
Interdisciplinary Center for Security, Reliability and Trust (SnT), Luxembourg, Luxembourg

LUIS D. EMILIANI, Senior Member, IEEE
Societe Europeenne des Satellites (SES), Betzdorf, Luxembourg

***Abstract*— THE past decades witnessed the application of adaptive coding and modulation (ACM) in satellite links. However, ACM technologies come at the cost of higher complexity when designing the network's carrier plan and user terminals. Accounting for those issues is even more important when the satellite link uses frequencies in Ka band and above, where the attenuation caused by tropospheric phenomena is a major concern. In this paper, we propose a solution for the inbound, i.e., return link, carrier plan sizing of very small aperture terminal (VSAT) networks. As tropospheric attenuation is a key factor, we present a mathematical problem formulation based on spatially correlated attenuation time series. Our proposed sizing scheme is formulated as a mixed integer linear programming (MILP) optimization problem. The numerical results for a test scenario in Europe show a 10 to 50% bandwidth improvement over traditional sizing methods for outage probabilities lower than 1%.**

***Index Terms*—ACM, VSAT, resource allocation, MILP optimization, spatially correlated fade**

This work is supported by the Luxembourg National Research Fund (FNR) – RELICA project, ref. 14610745. *(Corresponding author: C. Lacoste)*. All authors contributed equally.

Authors' addresses: C. Lacoste, W. A. Martins, S. Chatzinotas, Signal Processing and Communications (SigCom) research group, Interdisciplinary Center for Security, Reliability and Trust (SnT), Luxembourg, Luxembourg, E-mail: (clement.lacoste@uni.lu). L. D. Emiliani, Spectrum Management and Development Department, Societe Europeenne des Satellites (SES), Betzdorf, Luxembourg.

0018-9251 © 2022 IEEE

I. INTRODUCTION

For *satellite communication* (SatCom) systems, radio bandwidth is one of the most precious resources. Satellite payloads are designed to deliver services for a variety of applications, each associated with a target service level agreement and desired area of service. The amount of bandwidth required to deliver services whilst meeting the service level agreements can vary considerably, depending on the type of service provided, such as TV broadcast, video on demand, voice, and Internet. Since spectrum is limited by regulations, SatCom service providers strive to deliver services to their customers using as little bandwidth as possible. Bandwidth optimization is thus of paramount importance.

When optimizing bandwidth usage, we can distinguish two scales:

- Micro/real-time scale: in this case the optimization focuses on real-time bandwidth and time-slot allocation [1], with short-term impairments and traffic prediction [2]. Techniques such as connection admission control [3], channel estimation [4], power allocation [5], and *adaptive coding and modulation* (ACM) [6] fall into this category.
- Macro/system scale: in this case the optimization is done at a system level, dealing with long-term statistics of channel behavior, link budget outputs, and traffic variations. Optimization on this scale usually aims to reduce the cost per Gbps [7] by tweaking key satellite characteristics such as beam number, frequency reuse, and *signal-to-interference-plus-noise ratio* (SINR) [8], or using smart gateways and temporal/spatial availability [9].

One of most well-known system-scale optimization problems in the current literature is the throughput capacity optimization of both *high throughput satellites* (HTS) and upcoming *very high throughput satellites* (VHTS), with flexible payloads (especially for the forward link) [7], [10]. This kind of optimization works best before the satellite deployment, when the payload can still be modified ("Upstream" part of Fig. 1 [11], [12]).

The topic of our paper also falls into the system-scale category, but focuses on solving a different problem when the satellite is already deployed. Once in orbit the satellite's transponders will be used to provide space segment resources, such as bandwidth, to support service provider's broadband networks, each using a fraction of the satellite's spectrum (service providers are located in the "Downstream" part of Fig. 1). Each service provider's request will give rise to a different network design (or modification of an existing one), which will require its own optimization process. The network designers also have to take into account specific constraints, thus increasing the complexity of the optimization problem. Limitations currently found in the industry most notably include:

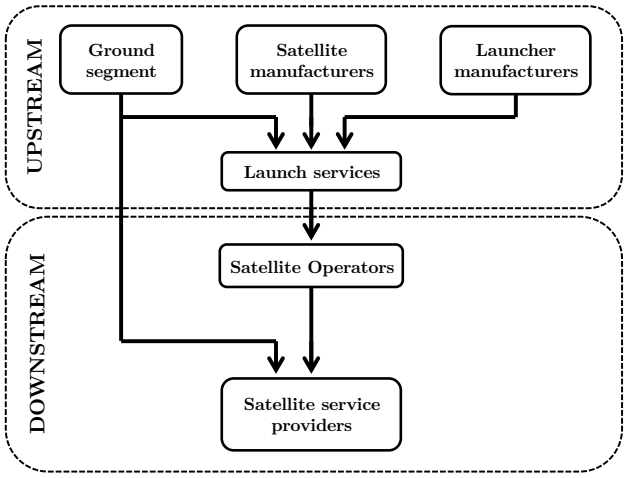

Fig. 1: Satellite revenue chain.

- Limited set of *modulation and coding* (ModCod) $\mathcal{M} = \{M_1, ..., M_K\}$, of carrier bandwidths $\mathcal{B} = \{B_1, ..., B_L\}$, of terminal power amplifier size, and of antenna gains. Such constraints are dictated by the product catalogue proposed by each service provider, and transform the sizing process in a combinatorial optimization problem.
- Not fully adaptive ACM networks, as in *adaptive return carrier selection* (ARCS) [13]. In this case, the return carriers are not allowed to adapt their ModCod or bandwidth to the fade conditions — user terminals can only select one of the pre-existing carriers. It is then necessary to establish a *carrier plan*, best described as a matrix $\mathbf{C}$, with its entries $c_{k,l}$ being the number of carriers associated with M_k and B_l.

Careful design of the carrier plan is an extremely important step of the design process. On the one hand, the carrier plan dictates the bandwidth B^{tot} used by the network via the following equation:

$$B^{\text{tot}} = \sum_{k=1}^{K} \sum_{l=1}^{L} c_{k,l} \cdot B_l \,. \qquad [\text{Hz}] \tag{1}$$

On the other hand, the carrier plan also dictates the throughput capacity of the network R^{tot} via the following equation:

$$R^{\text{tot}} = \sum_{k=1}^{K} \sum_{l=1}^{L} c_{k,l} \cdot B_l \cdot S_k \,, \qquad [\text{bps}] \tag{2}$$

where S_k denotes the spectral efficiency of M_k, in bps/Hz. Therefore, the carrier plan must also be designed to deliver the contractual *quality of service* (QoS) to the terminals, which can conflict with the bandwidth minimization. The design of the carrier plan is then a complex trade-off between bandwidth minimization and QoS satisfaction. The complexity is at its highest when designing the return link sizing of *very small aperture terminal* (VSAT) networks since: (i) the link budget is tighter in the return link compared to the forward link, thus the carrier types (ModCod and bandwidth size) are more heterogeneous in order to offer more options in case of fade; (ii) a potentially large number of terminals with stringent QoS requirements may be considered.

The primary goal of this paper is to determine what the optimal VSAT carrier frequency plan needs to be in order to both meet the QoS constraints and minimize the total bandwidth consumption. To the best of our knowledge, the problem of optimal inbound carrier plan design, and more generally return link sizing, in the adaptive VSAT context has not been satisfactorily addressed in the scientific literature nor in the industry. On the industry side, service providers use heuristics without optimality guarantees [14]–[16].

In the literature, the sizing of fade-adaptive satellite networks has been studied in [17] to demonstrate how time-series synthesizers can improve ACM network designs. The authors in [17] have generated a time series of rain maps using the MultiEXCELL rain field simulation model and have used them to determine the ModCod usage statistics. Using a long-term average approach, the authors have presented how to derive the necessary number of carriers and have shown how to build the *complementary cumulative distribution functions* (CCDF) of the number of carriers needed for each ModCod. However, one of the key questions left unaddressed by the authors is how to use such CCDFs to find the optimal carrier plan.

The authors of [18] have tried to answer this question. They have focused on using a *mixed integer linear programming* (MILP) formulation to optimize the carrier frequency plan, allowing to take into account hardware constraints such as a limited set of carrier bandwidths. However, the resulting MILP formulation falls short of providing a practical solution due to its inability to guarantee the QoS. The proposed solution also fails to take into account the spatial correlation of terminal's impairments, as the methodology focuses on individual terminal CCDFs and does not introduce correlation matrices. This work has inspired our previous work on optimizing inbound carrier plans for *constant coding and modulation* (CCM) networks [19].

In this paper, we expand the works in [17]–[19] with the following new contributions:

- A formal definition of the return link carrier plan sizing optimization problem using spatially correlated attenuation time series, from the input definitions to the identification of optimization variables and constraints.
- An MILP problem formulation which is solvable by standard solvers, as well as a comparison against classical sizing methods in a test scenario in Europe, using MultiEXCELL for the generation of tropospheric attenuation.

The paper is organized as follows. In Section II, we introduce the VSAT ACM scenario as well as the carrier plan definition. In Section III, we define the attenuation time

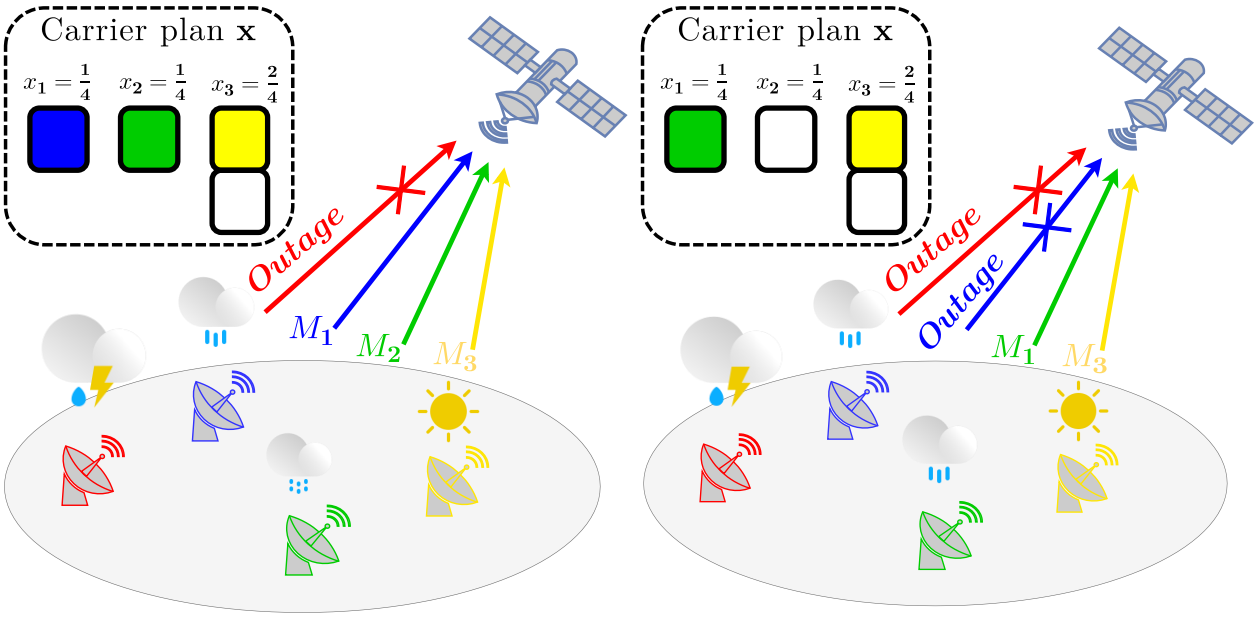

(a) Illustration of outage (red terminal) due to severe fade conditions.

(b) Illustration of outage (blue terminal) due to congestion at M_1.

Fig. 2: Illustration of the ModCod demand and carrier plan, with $N = 4$ terminals and $K = 3$ ModCods.

series along with other input parameters, and show how to formulate a general optimization problem. In Section IV, we present a reformulation of the optimization problem, solvable by MILP solvers, as well as a benchmark based on current methods found in the literature. In Section V, we introduce a test scenario in Europe, and we present numerical results comparing our MILP method to the benchmark. In Section VI, we discuss some aspects of the two methods and the corresponding results. Finally, Section VII concludes the paper.

Notation: Bold uppercase $\mathbf{C}$ denotes matrices, bold lowercase $\mathbf{x}$ denotes (row) vectors, calligraphic uppercase $\mathcal{M}$ denotes sets. $|\mathcal{M}|$ refers to the cardinality of set $\mathcal{M}$, and $\lceil \cdot \rceil$ refers to the ceiling operator. For the reader's convenience, Table III, p. 13, describes the key notations found in this paper.

II. SCENARIO

This section describes the context and the different assumptions made in this paper. We firstly present the carrier plan and the key constraints it is subject to. We then present simulators of spatially correlated tropospheric attenuation, and explain why they are relevant to the return link sizing problem.

A. VSAT inbound carrier plan

We consider the return link carrier sizing problem of a single-beam satellite network serving N VSAT terminals. We assume that all terminals require the same uplink services. We also consider that the following QoS inputs have been agreed upon or computed in previous design steps:

1) The *committed information rate* (CIR), R_{CI} (in kbps), which is the contractual minimum bitrate under which a terminal is considered in outage.
2) The target outage probability, p, which is the maximum fraction of time a terminal can be allocated a throughput lower than R_{CI}. It is mainly dependent on the fade margin of the link and the robustness of the carrier plan to congestion.

Our goal is to find a carrier plan that minimizes the network's required satellite transponder bandwidth while ensuring the QoS constraints are satisfied. Given a pool of ModCods available in the network $\mathcal{M} = \{M_1, ..., M_K\}$, and pool of bandwidths $\mathcal{B} = \{B_1, ..., B_L\}$, we defined in Section I a carrier plan as a matrix $\mathbf{C}$, with $c_{k,l}$ being the number of carriers associated with M_k and B_l. Since in [19] we have proposed a heuristics that, starting from a given proportion of terminals $x_k \in [0, 1]$ using ModCod M_k, allows to compute the optimal $c_{k,l}$ values, for all k and l, that minimize the total carrier plan bandwidth, then we will focus on computing the optimal x_k in this work. We interpret x_k as the *maximum proportion of terminals* the network will be able to serve the QoS with ModCod M_k. We then define the (simplified) carrier plan $\mathbf{x}$ as

$$\mathbf{x} = (x_1, \ldots, x_K)\,. \tag{3}$$

As the network uses ACM schemes, terminals will be able to request different ModCods over time. The request of a ModCod by a given terminal will be driven by the attenuation conditions at this terminal's location. Fig. 2a illustrates an example of the terminals' requests, with

$N = 4$ terminals and $K = 3$ ModCods. The yellow terminal is in clear sky and can use the most efficient ModCod. On the other hand, the blue and green terminals, experiencing moderate fade, can only close a link using more robust ModCods than that available in clear sky. Finally, the red terminal is facing severe fading and cannot close the link.

The carrier plan, however, will not be allowed to change over short periods of time. This configuration, also used in [18], is inspired from the ARCS technology. In Fig. 2, we also illustrated an example of such carrier plan with $\mathbf{x} = (x_1, x_2, x_3)$, where $x_1 = x_2 = \frac{1}{4}$ and $x_3 = \frac{2}{4}$. This carrier plan can then serve at best one terminal using M_1, one terminal using M_2, and two terminals using M_3, for a total of four terminals. We represented the terminal capacity for each ModCod with small boxes, where one box represents a capacity of one terminal, and the color inside the box represents the terminal using this capacity at this time instant. For instance, in Fig. 2a, the blue terminal is using M_1, the green terminal is using M_2, and the yellow terminal is using M_3. Only one terminal is able to use M_3, therefore half of the capacity provisioned for M_3 is unused. This unused capacity is represented as a blank box. With this approach, our work aims to find practical solutions to common cases in the industry where the assumption of fully flexible carrier plans does not hold because of technology limitations.

In this context, great care must be taken in the composition of the carrier plan to avoid congestion, i.e., to prevent too many user terminals requesting the same ModCod at the same time. It is expected that, given the spatial correlation characteristics of the fade, it is likely that at a given moment in time, certain carriers will experience higher demand than others, due to the number of terminals experiencing similar levels of total link degradation and only able to close links using those specific ModCods. Beyond a certain congestion level, terminals will be denied service. Fig. 2b illustrates such case, as the blue and green terminals, facing the same fade conditions, have to request M_1. However, the carrier plan $\mathbf{x}$, identical to Fig. 2a, can only afford one terminal using M_1, and consequently the blue terminal is dropped due to congestion. Furthermore, the acceptable proportion of time service is denied to a given terminal is limited by the outage probability p, as defined earlier. Thus, the spatial correlation of fade plays a critical role in the design of the carrier plan.

B. Simulators of spatially correlated attenuation

Over the past decades, satellite communication systems have explored unoccupied spectrum regions wherein wider bandwidths are available. Many recent satellites use Ku and Ka bands, and more tests are being conducted using the Q/V band [20], which are expected to be employed by future telecommunication satellites [21]. However, an increase in frequency also leads to an increase in the tropospheric attenuation of the radio signal, thus requiring more accurate models to enable a proper design of such communication systems [22].

While most generally accepted models have been integrated into the well-known ITU Recommendation Propagation series [23], the statistical models have been criticized [24] for not being designed to make predictions with high spatio-temporal resolution. To address this issue, time-series synthesizers of tropospheric fade, considering both time and spatial domains, have been developed [24]–[26]. While firstly only able to generate attenuation for short periods (few hours) and small scales (hundreds of km^2), newer models such as in [27] have increased the size of the space and time dimensions of the synthesized series, allowing continental scale simulations spanning multiple years. These breakthroughs have fostered the use of time series generators in the design of satellite communication networks [28].

The application of spatially correlated time-series synthesizers has been firstly explored for the forward link in [29]. This work has illustrated how time series generators could be used to compute network-scale statistics, key to enabling applications in network sizing. Joint terminal fade statistics have been used to compare ACM and *variable coding and modulation* (VCM) technologies in a multibeam video broadcast satellite scenario [30]. Their numerical simulations with the software SISTAR have shown that VCM performs better in the context of multibeam forward link broadcast.

The impact of fade correlation was found to be even more important on the inbound side. The impact on the Shannon capacity of multibeam return links has been thoroughly explored in [31]. The authors have used a statistical model of the rain fade correlation, similar to [26], in the modeling of the terminals' channels. From this model, the authors have shown how to deduce long-term CCDF of the network ergodic capacity in function of the outage probability, and have concluded that introducing spatially correlated rain attenuation results in a significant decrease in channel capacity.

In order to consider the spatial correlation of fade, we propose in this paper to take the time series of spatially correlated attenuations as an input of our design method.

III. PROBLEM FORMULATION

The outputs of a time-series synthesizer are the attenuation time series $a_n(t)$ faced by the terminal $n \in \{1, \ldots, N\}$ at time $t \in \{1, \ldots, T\}$. Knowing the satellite and ground stations characteristics, the SINR, $\left(\frac{C}{N+I}\right)_n(t)$, can then be computed through a link budget, as follows:

$$\left(\frac{C}{N+I}\right)_n(t) = \left[\frac{1}{\left(\frac{C}{N}\right)_n^{\mathrm{ul}}(t)} + \frac{1}{\left(\frac{C}{IM}\right)_n(t)} + \frac{1}{\left(\frac{C}{N}\right)_n^{\mathrm{dl}}(t)}\right]^{-1} \tag{4}$$

in which $\left(\frac{C}{N}\right)_n^{\mathrm{dl}}(t)$ is the downlink SINR of terminal n, $\left(\frac{C}{IM}\right)_n(t)$ is the carrier to intermodulation noise ratio,

and $\left(\frac{C}{N}\right)_n^{\mathrm{ul}}(t)$ is the uplink SINR, defined in dB as

$$\left(\frac{C}{N}\right)_n^{\mathrm{ul}}(t) = \mathrm{EIRP}_n^0 - L_n^{\mathrm{fs}} - a_n(t) + \left(\frac{G}{T}\right)_n^{\mathrm{sat}} - k_{\mathrm{B}} \quad [\mathrm{dB}]\,, \tag{5}$$

and where:

- EIRP_n^0 is the *equivalent isotropic radiated power* (EIRP) density of terminal n. We assume the terminals work in *power equivalent bandwidth* (PEB) mode, in which emission power is scaled with bandwidth.
- L_n^{fs} is the free space loss between terminal n and the satellite.
- $\left(\frac{G}{T}\right)_n^{\mathrm{sat}}$ is the figure of merit of the satellite at the location of terminal n.
- k_{B} is the Boltzmann constant.

Along the $\left(\frac{C}{N+I}\right)_n(t)$ time series, we assume the following additional parameters are given:

- The number of terminals N.
- The CIR R_{CI}, in kbps.
- The outage probability p.
- The set of ModCods $\mathcal{M} = \{M_1, \ldots, M_K\}$.
- The set of ModCod SNR activation thresholds $\Theta = \{\theta_0, \theta_1, \ldots, \theta_K\}$, with $\theta_0 = -\infty$.[1]
- The set of spectral efficiencies $\mathcal{S} = \{S_1, \ldots, S_K\}$, in bps/Hz. We assume S_k increases with θ_k.

The output of our optimization process will be the optimal carrier plan $\mathbf{x}^{\mathrm{opt}} \in [0,1]^K$, which minimizes the system bandwidth under the constraint that no terminal will be delivered a throughput inferior to R_{CI} for a proportion of time greater than p. For the sake of conciseness, we will refer to this constraint as the "outage constraint".

A. ModCod request time series

Before diving in the optimization problem, we first need to process the SINR time series in order to extract a time series of ModCod requests, which we can then use to find the optimal carrier plan. An illustration of the different steps is given in Fig. 3. After computing the SINR time series from the attenuation, the following step is to find the index $K_n(t)$ of the most spectrally efficient ModCod $M_{K_n(t)}$ that the terminal n can use at time t. This is done by comparing the terminal SINR, $\left(\frac{C}{N+I}\right)_n(t)$, against the ModCod thresholds in order to satisfy the following:

$$K_n(t) = \max\left\{k \in \{0,1,\ldots,K\} : \theta_k \leq \left(\frac{C}{N+I}\right)_n(t)\right\}. \tag{6}$$

We can then determine the ModCod request proportion time series, $\hat{x}_k(t)$, as follows:

$$\hat{x}_k(t) = \frac{|\{n \in \{1,\ldots,N\} \ : \ K_n(t) = k\}|}{N}\,, \tag{7}$$

for all $k \in \{1,\ldots,K\}$, and

$$\hat{\mathbf{x}}(t) = (\hat{x}_1(t), \ldots, \hat{x}_K(t))\ . \tag{8}$$

In this paper, we will use the hat notation to indicate that $\hat{x}_k(t)$ is a sample computed from the SINR time series. We also define λ_n, the proportion of samples in which terminal n is not able to close the link, as

$$\lambda_n = \frac{|\{t \in \{1,\ldots,T\} \ : \ K_n(t) = 0\}|}{T}\,. \tag{9}$$

We assume that, for any terminal n, λ_n is strictly less than p. Having this condition violated would mean the terminals have not been designed properly in early design steps, and no carrier plan will be able to satisfy the outage constraint.

From a given $\mathbf{x}$, we are able to compute the bandwidth needed to deliver R_{CI} to each of the terminal proportions x_k via

$$B(\mathbf{x}) = \sum_{k=1}^{K} \frac{x_k \cdot N \cdot R_{\mathrm{CI}}}{S_k} \quad [\mathrm{kHz}]\,. \tag{10}$$

Our goal is then to find the optimal carrier plan $\mathbf{x}^{\mathrm{opt}} = (x_1^{\mathrm{opt}}, ..., x_K^{\mathrm{opt}})$ such that:

$$\mathbf{x}^{\mathrm{opt}} = \arg\min_{\mathbf{x} \in \mathcal{O}} B(\mathbf{x})\,, \tag{11}$$

with $\mathcal{O} \subset [0,1]^K$ the viable set of carrier plans that satisfy the outage constraint, which we need to express mathematically.

B. Outage constraint through order relation

Let us assume we have found $\mathbf{x}^{\mathrm{opt}}$ and have selected it as our network carrier plan. Let us also assume that our network terminals meet fade conditions that lead to a ModCod demand equal to $\hat{\mathbf{x}}(t)$. In this scenario, the proportion of terminals requesting M_k is $\hat{x}_k(t)$. If x_k^{opt} is greater or equal to $\hat{x}_k(t)$, all the corresponding terminals will have their demand satisfied. However, if x_k^{opt} is less than $\hat{x}_k(t)$, the network's carrier plan will not be able to satisfy all terminals' demands. The remaining proportion of terminals $\hat{x}_k(t) - x_k^{\mathrm{opt}}$ will have to seek free capacity in other coordinates of $\mathbf{x}^{\mathrm{opt}}$, i.e., use another ModCod. As ModCod usage is conditioned by the terminal SINR, the remaining proportion of terminals can only be re-allocated to x_i^{opt} with $i \in \{1,\ldots,k-1\}$. Having a capacity allocated to every terminal requesting M_k at time t, including the remaining terminals, is then equivalent to having at least $\hat{x}_k(t) - x_k^{\mathrm{opt}}$ free capacity in the $k-1$ ModCods between M_1 and M_{k-1}, that is:

$$\sum_{i=1}^{k-1} x_i^{\mathrm{opt}} - \sum_{i=1}^{k-1} \hat{x}_i(t) \geq \hat{x}_k(t) - x_k^{\mathrm{opt}}\,. \tag{12}$$

By iterating on k, we deduce that all terminals able to close the link at time t can have a capacity allocated in $\mathbf{x}^{\mathrm{opt}}$ iff

$$\sum_{i=1}^{k} x_i^{\mathrm{opt}} \geq \sum_{i=1}^{k} \hat{x}_i(t) \qquad \forall k \in \{1,\ldots,K\}\,. \tag{13}$$

[1] The parameter θ_0 is used to generalize Eq. (6), and does not have a physical meaning.

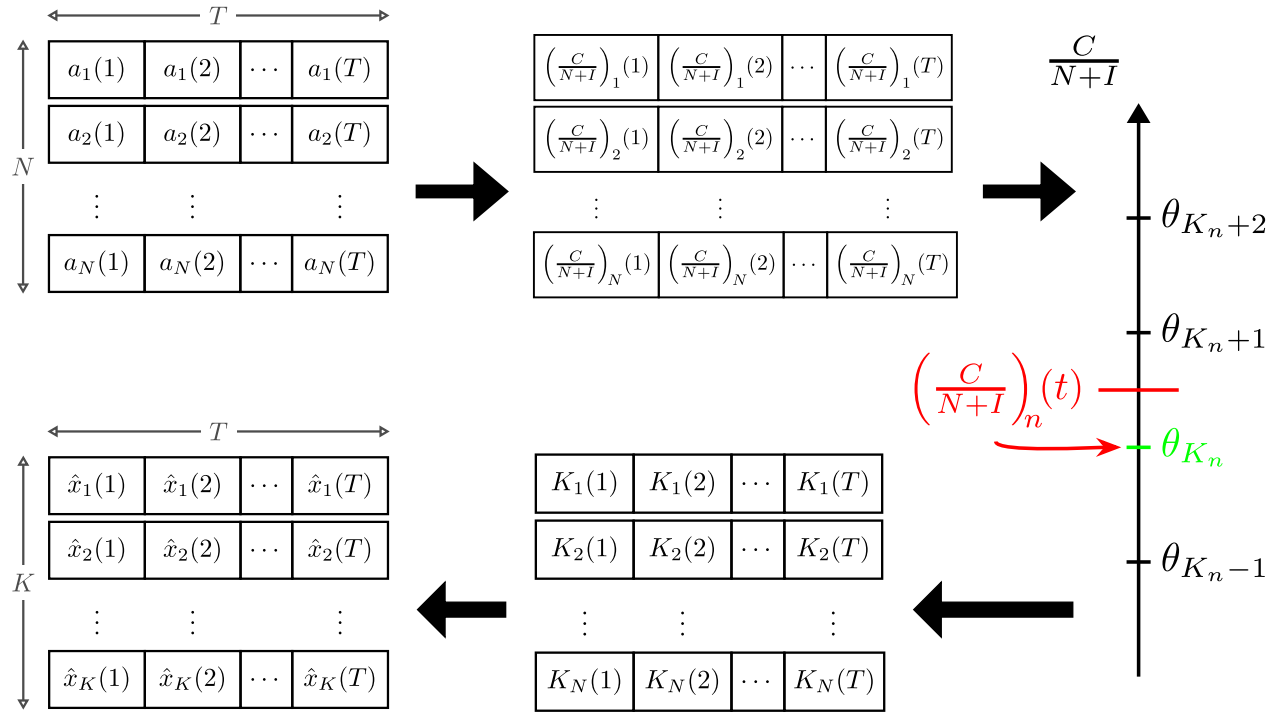

Fig. 3: Illustration of the calculation steps, from the attenuation time series $a_n(t)$ to the ModCod request time series $\hat{x}_k(t)$.

We then denote the order relation $\succeq$ as

$$\mathbf{x}^{\text{opt}} \succeq \hat{\mathbf{x}}(t) \Leftrightarrow \sum_{i=1}^{k} x_i^{\text{opt}} \geq \sum_{i=1}^{k} \hat{x}_i(t) \quad \forall k \in \{1,\dots,K\}\,, \tag{14}$$

and say that $\mathbf{x}^{\text{opt}}$ can accommodate $\hat{\mathbf{x}}(t)$. This relation is a partial order, but it is not a total order, as it is possible to have both $\mathbf{x}^{\text{opt}} \not\succeq \hat{\mathbf{x}}(t)$ and $\mathbf{x}^{\text{opt}} \not\preceq \hat{\mathbf{x}}(t)$, and thus $\mathbf{x}^{\text{opt}} \not\succeq \hat{\mathbf{x}}(t) \not\preceq \mathbf{x}^{\text{opt}}$. It is also different from the well-known majorization relation [32] since the vector's coordinates are not sorted in descending order.

Let $\mathcal{A}_{\mathbf{x}}$ denote the set containing all samples accommodated by $\mathbf{x} \in [0,1]^K$ as follows:

$$\mathcal{A}_{\mathbf{x}} = \{t \in \{1,\dots,T\} \;:\; \mathbf{x} \succeq \hat{\mathbf{x}}(t)\}\,. \tag{15}$$

If terminals could always close the link, we could ensure the satisfaction of outage constraint by designing $\mathbf{x}^{\text{opt}}$ such that no terminals will be dropped because of congestion for at least $\lceil T \cdot (1-p) \rceil$ samples. This is equivalent to have $\mathbf{x}^{\text{opt}}$ accommodating $\lceil T \cdot (1-p) \rceil$ samples, and is written as

$$|\mathcal{A}_{\mathbf{x}^{\text{opt}}}| \geq T \cdot (1-p)\,. \tag{16}$$

Note that (16) is more stringent on $\mathbf{x}^{\text{opt}}$ than the original outage constraint. It implicitly states that $\mathbf{x}^{\text{opt}}$ cannot drop even one terminal for at least $\lceil T \cdot (1-p) \rceil$ samples. For the remaining $\lfloor T \cdot p \rfloor$ samples, one or more terminals will be in outage, but it will likely not be the same terminals for every sample. Thus, even the highest outage statistic among terminals can be much lower than p in certain cases.

However, the terminals outages are not just due to congestion, but also to link outage. Let $\lambda^{\max}$ be the maximum proportion of time during which one terminal cannot close the link, that is:

$$\lambda^{\max} = \max\{\lambda_1,\dots,\lambda_N\}\,. \tag{17}$$

As we do not know when a terminal will have its link in outage, we need to assume that the set of time samples at which a terminal cannot close its link is disjoint from the set of time samples at which this terminal is dropped due to congestion. This implies that $\mathbf{x}^{\text{opt}}$ will have to accommodate not just $\lceil T \cdot (1-p) \rceil$ samples, but $\lceil T \cdot (1-p+\lambda^{\max}) \rceil$. The optimal carrier plan then has to satisfy

$$|\mathcal{A}_{\mathbf{x}^{\text{opt}}}| \geq T \cdot (1-p+\lambda^{\max})\,. \tag{18}$$

We can finally express $\mathcal{O}$ as:

$$\mathcal{O} = \left\{\mathbf{x} \in [0,1]^K \;:\; |\mathcal{A}_{\mathbf{x}}| \geq T \cdot (1-p+\lambda^{\max})\right\}\,, \tag{19}$$

and therefore rewrite (11) as the following optimization problem:

$$\begin{aligned} \underset{\mathbf{x}}{\text{minimize}} \quad & B(\mathbf{x}) && \text{(20a)}\\ \text{subject to} \quad & |\mathcal{A}_{\mathbf{x}}| \geq T \cdot (1-p+\lambda^{\max}) && \text{(20b)}\\ & \mathbf{x} \in [0,1]^K && \text{(20c)} \end{aligned}$$

IV. OPTIMIZATION FORMULATION

The main difficulty in solving (20) resides in efficiently determining if a given $\mathbf{x}$ satisfies (20b). In this section, we reformulate (20b) with integer constraints, enabling the use of MILP solvers. Then, we introduce

a worst-case method that we will compare against our MILP formulation in Section V.

A. Mixed integer linear programming

The optimization problem (20) is quite difficult to solve due to the cardinality constraint on $\mathcal{A}_{\mathbf{x}}$ in (18), which is non-linear. Drawing inspiration from the work in [33], we can translate the cardinality constraint into an integer constraint. This is done by introducing a binary optimization variable, $\boldsymbol{\alpha} \in \{0,1\}^T$, as in (21) at the bottom of p. 7. This variable lets the solver decide which samples should be accommodated by $\mathbf{x}$. We can then rewrite the cardinality-constrained optimization problem (20) as the MILP optimization problem (22) (bottom of p. 7). This formulation is solvable by standard MILP solvers. The number of constraints grows as $\mathcal{O}(K+T)$, as does the size of the optimization variables.

It is important to note that T is implicitly linked to $p-\lambda^{\max}$. Indeed, as we previously stated, we are looking for a solution that satisfies (20b). As we have assumed that $\lambda_n < p$ for all $n \in \{1,\dots,N\}$, then $p-\lambda^{\max} \in [0,1]$; thus, there exists some $z \in \{0,\dots,T-1\}$ such that $\frac{z}{T} \leq p-\lambda^{\max} < \frac{z+1}{T}$. Hence, (20b) is equivalent to:

$$\begin{aligned} & |\mathcal{A}_{\mathbf{x}^{\text{opt}}}| \geq T\cdot(1-p+\lambda^{\max}) \\ \iff & |\mathcal{A}_{\mathbf{x}^{\text{opt}}}| \geq \lceil T\cdot(1-p+\lambda^{\max})\rceil \\ \iff & |\mathcal{A}_{\mathbf{x}^{\text{opt}}}| \geq T-z\,. \end{aligned} \tag{23}$$

In the particular case where p is so small that $0 \leq p-\lambda^{\max} < \frac{1}{T}$, then from (23) and the fact that $|\mathcal{A}_{\mathbf{x}^{\text{opt}}}| \leq T$ we would have

$$|\mathcal{A}_{\mathbf{x}^{\text{opt}}}| \geq T\cdot(1-p+\lambda^{\max}) \iff |\mathcal{A}_{\mathbf{x}^{\text{opt}}}| = T\,. \tag{24}$$

In this case, the solver has to find a solution that accommodates every sample, and it will output the same solution regardless of the value of p. However, as one can see in Fig. 4 in p. 8, the rain attenuation CCDF, and subsequently the total attenuation, grows exponentially with $\log(1-p)$. This exponential behavior has an impact on the size of the bandwidth used by the optimal carrier plan. Thus, having $0 \leq p-\lambda^{\max} < \frac{1}{T}$ is an issue, as the bandwidth required to accommodate all samples might be much bigger than what would be really needed for this value of p. In order to not oversize our carrier plan for a given p value, we then need to make sure that $T \geq \frac{1}{p-\lambda^{\max}}$.

B. Worst-case method

As benchmark for our proposal, we consider a worst-case approach, which is simpler and does not consider the spatial correlation of fade. At worst, all terminals are always under fade simultaneously. Under this assumption, finding the optimal *worst-case* carrier plan $\mathbf{x}^{\text{wc}}$ is simpler, as the outage constraint is now only dictated by the link outage probability. The composition of $\mathbf{x}^{\text{wc}}$ can be determined by finding, for each terminal n, the ModCod that will provide a link outage probability smaller than p. Traditional network sizing methods would achieve this by following the ITU recommendations and compute the attenuation CCDF for each terminal individually. Then, the CCDF is used to compute the corresponding SINR, and in turn select the ModCod that will guarantee continuous operations at the fade levels corresponding to p. This method is commonly used in the satellite network dimensioning literature [7], [10].

In our method, we already computed time series of SINR. We can then define the empirical SINR CDF of each terminal n across time as

$$F_n^{\text{SINR}}(y) = \frac{\left|\left\{t\in\{1,\dots,T\} \;:\; \left(\frac{C}{N+I}\right)_n(t) < y\right\}\right|}{T} \tag{25}$$

for all $n \in \{1,\dots,N\}$ and $y \in \mathbb{R}_+$, in dB. The value of $F_n^{\text{SINR}}(y)$ is the proportion of samples in which the SINR of terminal n falls below the value y. We can then compute $\left(\frac{C}{N+I}\right)_n^{\text{wc}}$, the worst SINR met by terminal n with an outage probability p, with the generalized inverse

$$|\mathcal{A}_{\mathbf{x}}| \geq T\cdot(1-p+\lambda^{\max}) \iff \begin{cases} \sum_{i=1}^{k} x_i \geq \alpha_t \cdot \sum_{i=1}^{k} \hat{x}_i(t) & \forall k\in\{1,\dots,K\}, \forall t\in\{1,\dots,T\} \\ \sum_{t=1}^{T} \alpha_t \geq T\cdot(1-p+\lambda^{\max}) \end{cases} \tag{21}$$

$$\begin{aligned} \underset{\mathbf{x},\boldsymbol{\alpha}}{\text{minimize}} \quad & B(\mathbf{x}) && && \text{(22a)} \\ \text{subject to} \quad & \sum_{i=1}^{k} x_i \geq \alpha_t \cdot \sum_{i=1}^{k} \hat{x}_i(t) && \forall k\in\{1,\dots,K\}, \forall t\in\{1,\dots,T\} && \text{(22b)} \\ & \sum_{t=1}^{T} \alpha_t \geq T\cdot(1-p+\lambda^{\max}) && && \text{(22c)} \\ & \mathbf{x} \in [0,1]^K && && \text{(22d)} \\ & \boldsymbol{\alpha} \in \{0,1\}^T && && \text{(22e)} \end{aligned}$$

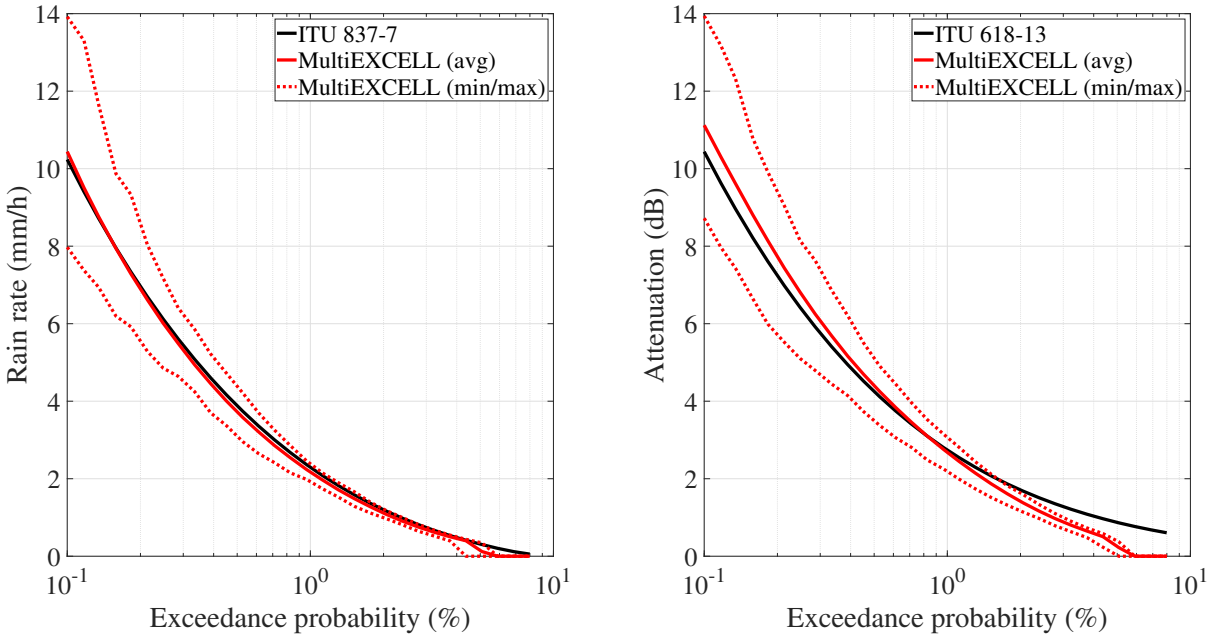

(a) Rain rate CCDF

(b) Rain attenuation CCDF

Fig. 4: Complementary CDFs of (a) rain rate and (b) rain attenuation, averaged over terminals, obtained with ITU-R P.837-7 (black solid curve) and with the MultiEXCELL samples (red solid curve), as well as minimum and maximum (resp. min/max red dotted curves) CCDFs across all terminals obtained with MultiEXCELL samples.

distribution function $(F_n^{\mathrm{SINR}})^{-1}(p)$, that is:

$$\left(\frac{C}{N+I}\right)_n^{\mathrm{wc}} = (F_n^{\mathrm{SINR}})^{-1}(p) = \inf\left\{y \in \mathbb{R}_+ \ : \ F_n^{\mathrm{SINR}}(y) \geq p\right\}. \tag{26}$$

We can then find the ModCod index $K_n^{\mathrm{wc}} \in \{1, \ldots, K\}$ such that

$$K_n^{\mathrm{wc}} = \max\left\{k \in \{1, \ldots, K\} \ : \ \theta_k \leq \left(\frac{C}{N+I}\right)_n^{\mathrm{wc}}\right\}. \tag{27}$$

We finally have our worst-case carrier plan solution:

$$x_k^{\mathrm{wc}} = \frac{|\{n \in \{1, \ldots, N\} \ : \ K_n^{\mathrm{wc}} = k\}|}{N}, \tag{28}$$

for all $k \in \{1, \ldots, K\}$.

V. NUMERICAL RESULTS

In this section, we compare the MILP method, proposed in Section IV-A, with the worst-case method, described in Section IV-B. We firstly present the test scenario and parameters. We then compare the bandwidth produced by the carrier plans, B^{milp} and B^{wc}, respectively computed using the MILP and the worst-case methods.

A. Test scenario

For our test scenario, we selected a Ka beam in Europe. We generated 489 rain maps of 200 by 200 km centered on (50.79°N, 7.87°E) with the MultiEXCELL model. In addition, $N = 500$ terrestrial terminals were generated in the same area based on the population density data of SEDAC [34] (see Fig. 5). For this paper, we focused only on the rain component of the tropospheric attenuation, as it is expected to be its dominant contribution. Figs. 4a and 4b respectively show the rain rate and the rain attenuation CCDFs obtained with such method for $T = 30,000$ MultiEXCELL maps, with solid lines representing averages and dotted lines representing minimums/maximums amongst terminals. On average, the synthetic curves are close to the ITU curves. The differences among the attenuation curves are due to the methods used to compute the attenuation from the rain rate. For the MultiEXCELL maps, we used the ATM PROP method [35], which differs slightly from the ITU Recommendation P.618 [36].

Other link parameters are given in Table I. As for the computation of the terminals' return link total SINR in (4), as we use a single beam, the term $\left(\frac{C}{IM}\right)_n(t)$ is expected to be relatively high. In addition, considering a star topology network, the downlink SNR $\left(\frac{C}{N}\right)_n^{\mathrm{dl}}(t)$ from the satellite to the gateway is also expected to be relatively high, assuming no fade on this link. On the other hand, $\left(\frac{C}{N}\right)_n^{\mathrm{ul}}(t)$ is expected to be relatively small due to limitations on the terminals' antenna size and amplifier power. Under those assumptions, the terminals' return link total SINR is therefore driven by the uplink SNR, such

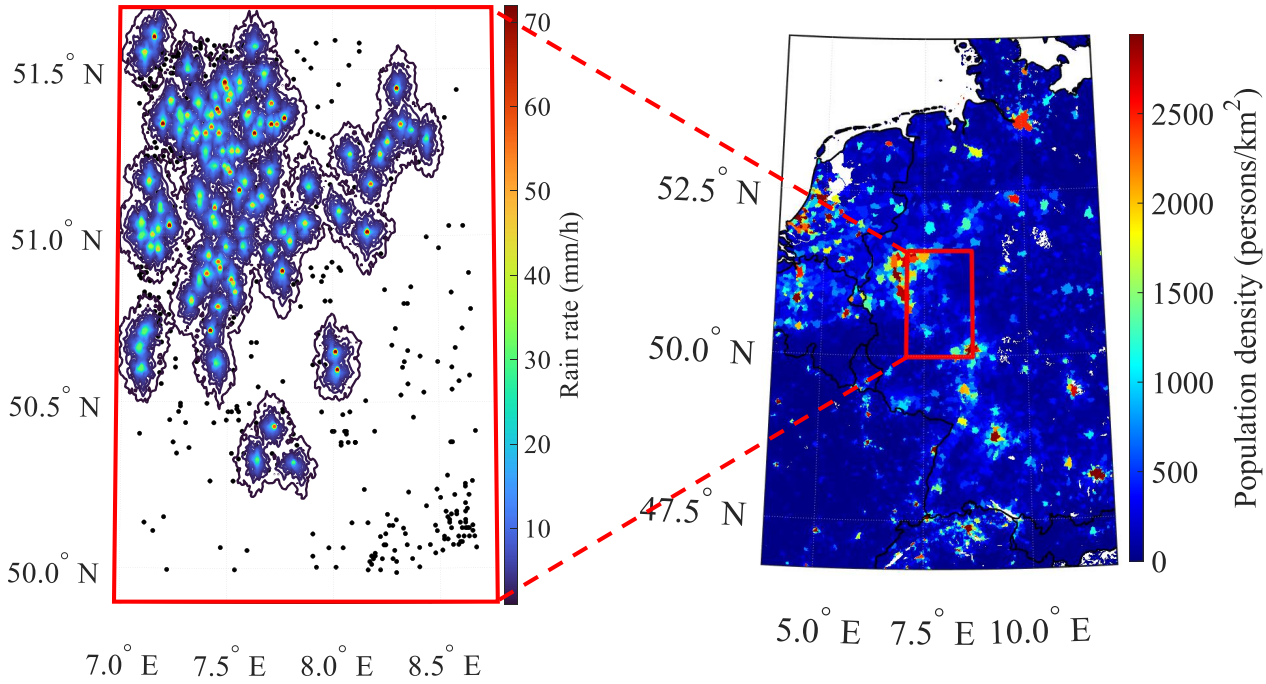

Fig. 5: Population density used for the terminal generation (right, inside red rectangle) as well as rain map example (left) over generated terminals (black dots)

TABLE I: Simulation link parameters

Name	Value	Unit
Frequency	29.75	GHz
Terminals antenna diameter	0.85	m
Terminals antenna gain	45.6	dBi
Satellite Longitude	28.5	°East
Average Satellite $\frac{G}{T}$	14.8	dB/K

TABLE II: DVB-RCS2 ModCod parameters

Modulation	Code rate	Spectral efficiency	Required $\frac{E_s}{N_0}$
QPSK	1/3	0.54	0
QPSK	1/2	0.83	2.3
QPSK	2/3	1.16	3.9
QPSK	3/4	1.31	5
QPSK	5/6	1.47	6.1
8-PSK	2/3	1.57	8.2
8-PSK	3/4	1.76	9.3
8-PSK	5/6	1.96	11
16-QAM	3/4	2.31	11.6
16-QAM	5/6	2.57	13

that:

$$\left(\frac{C}{N+I}\right)_n(t) \approx \left(\frac{C}{N}\right)_n^{\text{ul}}(t)\,. \tag{29}$$

We selected a maximum information rate of 1 Mbps and a 1:50 contention ratio as suggested in [37], giving us $R_{\text{CI}} = 200$ kbps. We used a ModCod set based on the DVB-RCS2 standard [38]. The ModCod SNR thresholds and spectral efficiencies, shown in Table II ($K = 10$), are extracted from [39, Table III].

Our results will show the evolution of both methods' performances across different values of $p \in [p^{\min} = 1 \cdot 10^{-3}, p^{\max} = 5 \cdot 10^{-2}]$. As the sizing of EIRP^0 depends on the uplink rain margin, and thus on p, two different approaches were followed:

- One where EIRP^0 is designed to ensure that the terminal with the most stringent link-budget in clear sky is able to afford the less demanding ModCod, M_1, with an uplink rain margin equal to $\max_n A_n(p^{\min})$. Under this condition, the value of EIRP^0, and consequently, $\lambda^{\max}$, does not depend on the actual value of p. Thus, the closer p is to $p^{\max}$, the bigger $p - \lambda^{\max}$ becomes, and the terminals' transmission capabilities might be oversized. While this approach minimizes bandwidth costs, it maximizes the terminals' equipment cost (amplifier and antenna), and the total network cost might

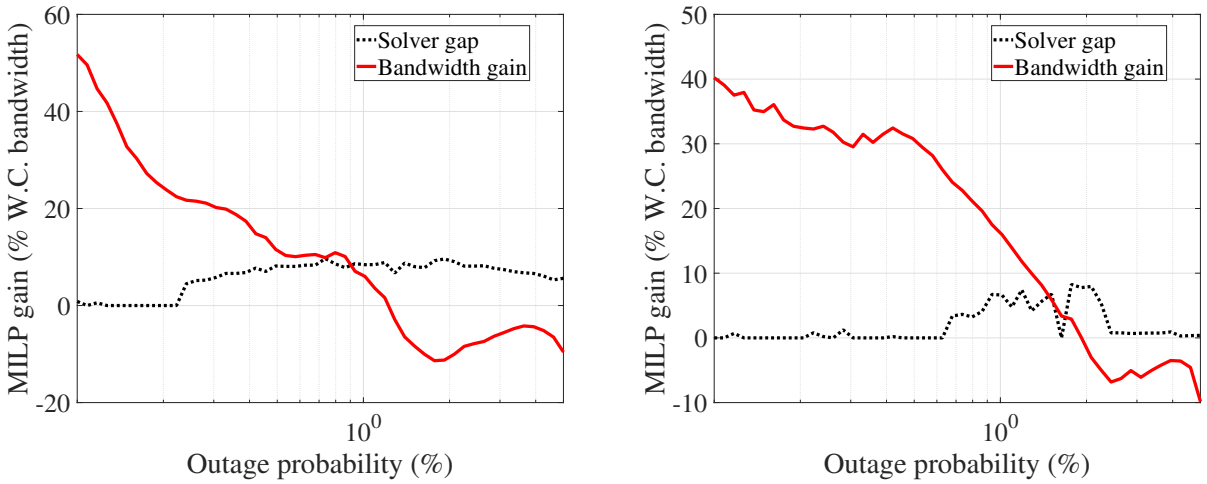

(a) Bandwidth gain and solver gap, BOE

(b) Bandwidth gain and solver gap, EOB

Fig. 6: Relative bandwidth gain $(B^{\mathrm{wc}} - B^{\mathrm{milp}})/B^{\mathrm{wc}}$ and solver gap $(B^{\mathrm{milp}} - B^{\mathrm{lb}})/B^{\mathrm{milp}}$ in function of p with (a) BOE and (b) EOB scenarios.

be sub-optimal. We will refer to this approach as *bandwidth over equipment* (BOE).

- A second one where EIRP^0 is re-computed at each given p to ensure that the terminal with the most stringent link-budget in clear sky is able to afford M_1, with an uplink rain margin equal to $\max_n A_n(p)$. Under this condition, the values of EIRP^0 and $\lambda^{\max}$ depend on the actual value of p, and the difference $p - \lambda^{\max}$ stays (almost) the same across all values of p. This approach minimizes equipment costs, but maximizes bandwidth costs. We will refer to this approach as *equipment over bandwidth* (EOB).

In a real network design, we expect that the bandwidth performances of our solution will fall in-between the results that are shown in the following sections.

In all scenarios, the value of $\lambda^{\max}$ never exceeded $9.65 \cdot 10^{-4}$. Thus, to satisfy the condition $T \geq \frac{1}{p-\lambda^{\max}}$, the 489 maps were circularly shifted multiple times in all directions across the area to obtain a number of time samples $T = 30,000$.

B. Bandwidth performance

As depicted by the red curves in Fig. 6, the relative bandwidth gain of B^{milp} w.r.t. B^{wc}, i.e., $(B^{\mathrm{wc}} - B^{\mathrm{milp}})/B^{\mathrm{wc}}$, increases when p decreases, and becomes significant (greater than 10%) for $p \leq 1\%$ in both scenarios. In both figures, the gain is negative for high p values (not commonly seen in VSAT networks). Then, it rapidly increases to positive values in the EOB scenario, while the increase is slower in the BOE scenario. We then conclude that oversizing the uplink equipment will decrease the potential gain the MILP method offers over the worst-case method.

As many simulations had to be run, we imposed a time limit on the MILP solving. The consequence is that for some values of p, the solver was not able to find the optimal integer value. The black dotted curves in Fig. 6 represent the relative gap, $(B^{\mathrm{milp}} - B^{\mathrm{lb}})/B^{\mathrm{milp}}$, between the bandwidth of the MILP solver's solution and the relaxed problem lower bound B^{lb}. We observe that the gap curve is overall higher for the BOE scenario than for the EOB scenario. Thus, finding an actual minimum is likely to take more time when the uplink is oversized. However, a positive gap value does not necessarily imply that a better point exists, but rather that not all options have been explored. Simulations for specific p values with longer time limits tend to show a reduction in gap due to finding a higher B^{lb} rather than finding a more bandwidth efficient solution.

The micro-variations in gain observed in Fig. 6 are mainly due to the variations of B^{wc}, represented by a black solid line in Figs. 7a and 7b. While B^{wc} follows a highly non-linear trend, B^{milp} shows an approximately linear behavior. We can then predict larger gains for outage probabilities lower than the ones showed. However such probabilities are currently rarely used for the design of VSAT return links, and generating a solution would require a much larger number of samples.

C. Worst terminal outage

While the MILP method showed overall promising bandwidth performances, it is also important to verify the satisfaction of the outage probability constraint. To this end, we created a test algorithm that determines, for each sample $\hat{\mathbf{x}}(t)$, which terminal will be dropped. For a given sample, the decision to drop terminal n is made by comparing $\left(\frac{C}{N+I}\right)_n(t)$ to $\left(\frac{C}{N+I}\right)_n^{\mathrm{wc}}$ and the

This article has been accepted for publication in IEEE Transactions on Aerospace and Electronic Systems. This is the author's version which has not been fully edited and content may change prior to final publication. Citation information: DOI 10.1109/TAES.2022.3194502

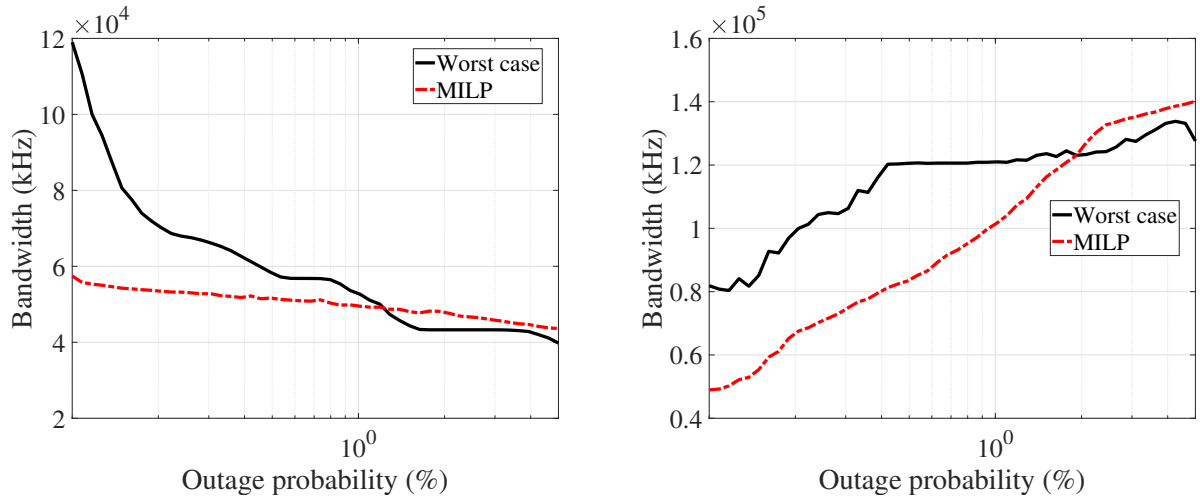

(a) B^{milp} and B^{wc}, BOE

(b) B^{milp} and B^{wc}, EOB

Fig. 7: Evolution of B^{milp} and B^{wc} in function of p with (a) BOE and (b) EOB scenarios.

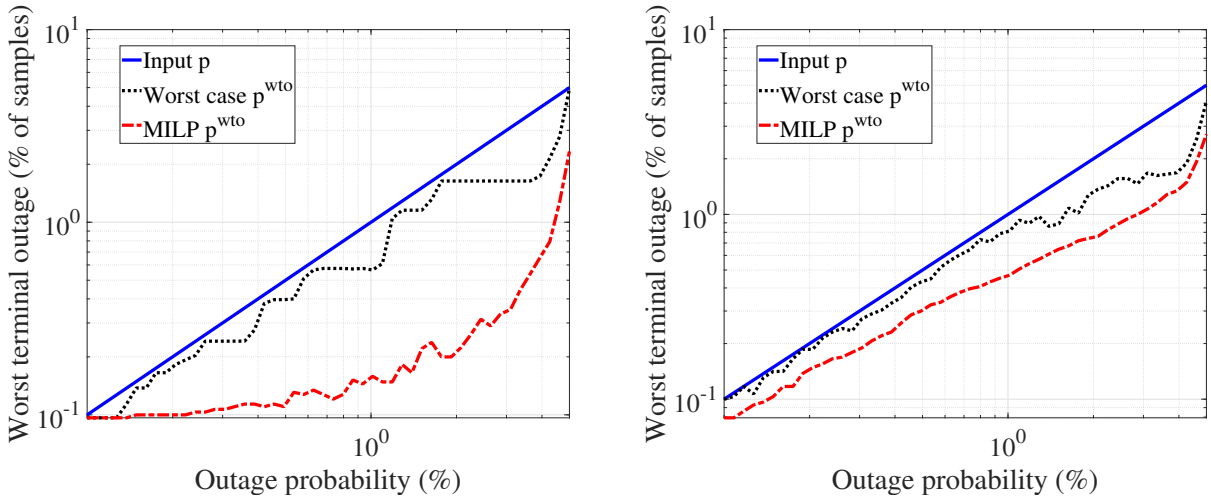

(a) Worst terminal outage p^{wto}, BOE

(b) Worst terminal outage p^{wto}, EOB

Fig. 8: Comparison of p^{wto} for worst case and MILP methods in function of requested p, with (a) BOE and (b) EOB scenarios.

terminal's clear sky SINR. Terminals are dropped until the inequality in (13) is satisfied. Once $\mathbf{x}^{\mathrm{opt}}$ has been compared against all samples, the algorithm returns the highest outage proportion (link outage + drop due to congestion) amongst terminals. We will name this value the worst terminal outage p^{wto}, and we expect $p^{\mathrm{wto}} \leq p$.

Fig. 8 shows the p^{wto} obtained when testing the carrier plans produced by both methods. We can see that both the MILP and the worst-case methods are able to satisfy $p^{\mathrm{wto}} \leq p$. Moreover, our MILP method provides lower p^{wto} than the worst-case method. It is then apparent that increasing the bandwidth efficiency of the solution does not necessarily come at the expense of higher outage probability. The gap between the two methods is quite significant in the BOE scenario, while moderate in the EOB scenario. We conclude that oversizing the uplink equipment has an impact on the oversizing of the MILP carrier plan.

VI. DISCUSSIONS

A. MILP solver implementation

The gain of the MILP method depends on the solver's implementation and parameters. In our case, we used the integrated MATLAB integer linear programming solver *intlinprog* [40]. We limited the solver's execution in time to 6 hours per value of p, with simulations running in parallel on single core threads. We also instructed the solver to stop if it found an integer solution within 1% of the relaxed solution, as gains lower or equal to 1% will not

be significant in the context of network cost optimization. Execution times of several hours are affordable in our problem as we are doing long term network planning. We also tested other solvers in specific scenarios, most notably SCIP [41] and CVX [42]. No notable differences in bandwidth gain or solver gap were observed with those parameters. However, we observed quicker reduction in the solver's gap when running a specific simulation on multiple cores with CVX.

B. Variability of rain

In Fig. 6, we observed a crossing point at which the MILP bandwidth increased from negative values to positive ones. This crossing point depends on the average annual probability of rain p_0 across terminals. As p_0 depends on the terminals' geographical locations, we expect the crossing point to change for networks serving tropical or desertic regions, where p_0 is respectively higher and lower than in our European scenario.

The number of samples T also plays a role in the variability of rain amongst terminals. The lower the exceedance probability is, the lower the number of samples representing this probability is. As shown in Fig. 4, this translates into a high variability among terminals' CCDFs at low exceedance probabilities. Higher T values would reduce this effect and bring the dotted curves in Fig. 4 closer to the average curves.

The variability of rain amongst terminals is also impacted by the geographical separation between terminals in the network. In our scenario, we used 200 by 200 km maps, as MultiEXCELL does not allow for the generation of much larger fields. The consequence is that the variability of rain is rather low, and mainly tied to T. Expanding the network size would bring more variability, and could change the performances of both methods. In future works, we plan to use different time series generators that span over larger areas, such as SISTAR.

C. Terminal drop policy

The curves shown in Fig. 8 depend on the terminal drop policy, of which an example was presented in Section V-C. One important property of this policy is that it stops dropping terminals when the accommodation property is satisfied. Thanks to the conservative nature of the accommodation property, the MILP method will guarantee $p^{\mathrm{wto}} \leq p$ for any dropping policy that satisfies the accommodation property. On the other hand, the worst-case method does not satisfy it; indeed, it can be straightforwardly verified by testing the resulting carrier plan on a drop policy which drops the terminals based on a pre-determined order, regardless of their SINR.

D. Heterogeneity for QoS and number of terminals

In a real VSAT network, it is common to have different QoS parameters (R_{CI} and p) among terminals. In this context, a way to use our technique would be to group terminals under QoS groups, run the optimization for each group separately, and then merge the resulting carrier plans. This approach, however, has no optimality guarantees. Having an optimization problem able to deal with heterogeneous QoS requirements remains an open problem to be addressed in future works.

Another concern is the disparity in the number of terminals between the design stage and deployment phase, as well as its increase during the network lifetime. If the number of terminals was overestimated during the design phase, then the carrier plan is still valid, although not optimal. On the other hand, if the number of terminals was underestimated, there will be more congestion than anticipated, and the QoS might not be achieved. As we already optimize the carrier plan for space-correlated fade, we expect our solution to be quite sensitive to an increase in the number of terminals. Therefore, real applications of our solution will likely have to anticipate a future rise in the number of terminals, and take margins accordingly.

VII. CONCLUSION

In this paper, we presented the carrier plan sizing problem for adaptive VSAT return links, and proposed a more bandwidth-efficient solution compared to current sizing methods. We defined the return link carrier plan design problem as applicable to broadband networks with adaptive return links, and proposed an MILP optimization formulation that explicitly accounts for the spatial correlation of the tropospheric fade, using time series generators. Finally, we introduced a sizing method commonly used in the literature, and compared it to our MILP method in a realistic test scenario.

The numerical results illustrated how the proposed MILP method brings a bandwidth improvement between 10% and 50% for outage probabilities less than 1%, whilst also being able to provide lower outage time than the benchmark method

From those results, we concluded that the MILP method can improve the sizing of adaptive VSAT inbounds by reducing their cost and providing stronger QoS guarantees. Future works will focus on introducing hardware constraints such as the terminals' power and antenna gain, and expand future test scenarios in scale and complexity (e.g., by introducing interference).

TABLE III: Glossary

Symbol	Unit	Name
Indexes		
n	N/A	User terminal index, $n \in \{1, \dots, N\}$
k	N/A	ModCod index, $k \in \{1, \dots, K\}$
t	N/A	Time sample index, $t \in \{1, \dots, T\}$
Variables		
R_{CI}	kbps	Committed information rate
p	N/A	Outage probability
M_k	N/A	ModCod with index k
θ_k	dB	SNR threshold of M_k, with $\theta_0 = -\infty$
S_k	bps/Hz	Spectral efficiency of M_k
$\mathbf{x}$	N/A	Return link carrier plan, $\mathbf{x} = (x_1, \dots, x_K) \in [0,1]^K$
x_k	N/A	Maximum proportion of terminals allowed to use M_k simultaneously
$a_n(t)$	dB	Attenuation met by terminal n at time t
$\left(\frac{C}{N+I}\right)_n(t)$	dB	SINR of terminal n at time t
$K_n(t)$	N/A	Index of the most efficient ModCod usable by terminal n at time t $\theta_{K_n(t)} \leq \left(\frac{C}{N+I}\right)_n(t) < \theta_{K_n(t)+1}$
$\hat{x}_k(t)$	N/A	Sample of the proportion of terminals requesting M_k at time t
λ_n	N/A	Proportion of time samples in which terminal n cannot close the link.
Sets		
$\mathcal{A}_{\mathbf{x}}$	N/A	Set of $\hat{\mathbf{x}}(t)$ subject to $\mathbf{x} \succeq \hat{\mathbf{x}}(t)$
$\mathcal{O}$	N/A	Set of $\mathbf{x} \in [0,1]^K$ satisfying (18)
Functions		
$B(\mathbf{x})$	kHz	Bandwidth occupation resulting from delivering R_{CI} to all terminals' slots in $\mathbf{x}$
$F_n^{\mathrm{SINR}}(y)$	N/A	Cumulative distribution function of the SINR of terminal n
Relations		
$\mathbf{x} \succeq \mathbf{x}'$	N/A	$\mathbf{x}$ accomodates $\mathbf{x}'$, $\mathbf{x} \succeq \mathbf{x}' \iff \forall k \in \{1, \dots, K\}, \ \sum_{i=1}^{k} x_i \geq \sum_{i=1}^{k} \mathbf{x}'_i$

ACKNOWLEDGMENT

We would like to thank Dr. Nicola Maturo for providing help and support during the early phases of this project. We would also like to thank Prof. Lorenzo Luini from Politecnico di Milano for providing the MultiEXCELL maps as well as precious help on the rain fade computations. Finally, we would like to thank Mr. Tedros Salih, who helped us with the MILP formulation.

References

[1] M. Al-Mosawi, R. Khusainov, and B. Gremont, "A real time algorithm for bandwidth and time-slot assignment for rain faded DVB-RCS systems," in *Fourth International Conference on Advances in Satellite and Space Communications*, Apr. 2012.

[2] A. Aroumont, J. Radzik, M. Bousquet, and L. Castanet, "DVB-RCS return link radio resource management for broadband satellite systems using fade mitigation techniques at Ka band," in *2008 IEEE International Workshop on Satellite and Space Communications*, Nov. 2008, pp. 221–225. DOI: 10.1109/IWSSC.2008.4656792.

[3] F. Tra, "Contrôle d'admission des connexions pour les systèmes de télécommunications par satellite avec des liaisons physiques adaptatives," Ph.D. dissertation, Institut Supérieur de l'Aéronautique et de l'Espace (ISAE), 2008.

[4] S. Cioni, R. De Gaudenzi, and R. Rinaldo, "Adaptive coding and modulation for the reverse link of broadband satellite networks," in *IEEE Global Telecommunications Conference, 2004. GLOBECOM '04.*, vol. 2, 2004, 1101–1105 Vol.2. DOI: 10.1109/GLOCOM.2004.1378128.

[5] M. Guerster, J. Jose Garau Luis, E. Crawley, and B. Cameron, "Problem representation of dynamic resource allocation for flexible high throughput satellities," in *2019 IEEE Aerospace Conference*, 2019, pp. 1–8. DOI: 10.1109/AERO.2019.8741398.

[6] H. Bischl, H. Brandt, T. de Cola, *et al.*, "Adaptive coding and modulation for satellite broadband networks: From theory to practice," *International Journal of Satellite Communications and Networking*, vol. 28, pp. 59–111, Jan. 2010. DOI: 10.1002/sat.932.

[7] F. G. Ortiz-Gomez, R. Martínez, M. A. Salas-Natera, A. Cornejo, and S. Landeros-Ayala, "Forward link optimization for the design of VHTS satellite networks," *Electronics*, vol. 9, no. 3, Mar. 2020, ISSN: 2079-9292. DOI: 10.3390/electronics9030473. [Online]. Available: https://www.mdpi.com/2079-9292/9/3/473.

[8] A. Cornejo, S. Landeros-Ayala, R. Martínez, and J. M. Matías, "Analysis to quantify and optimize spot beams for a high throughput satellite in Ka and Q/V bands," *IEEE Latin America Transactions*, vol. 17, no. 02, pp. 219–227, 2019. DOI: 10.1109/TLA.2019.8863167.

[9] N. Jeannin, L. Castanet, J. Radzik, M. Bousquet, B. Evans, and P. Thompson, "Smart gateways for terabit/s satellite," *International Journal of Satellite Communications and Networking*, vol. 32, Mar. 2014. DOI: 10.1002/sat.1065.

[10] D. Serrano-velarde, E. Lance, H. Fenech, and G. E. Rodriguez-guisantes, "Novel dimensioning method for high-throughput satellites: Forward link," *IEEE Transactions on Aerospace and Electronic Systems*, vol. 50, no. 3, pp. 2146–2163, Jul. 2014. DOI: 10.1109/TAES.2014.120429.

[11] V. Omelyanenko, "Basics of optimization strategy for integrating space industry technology package into global value chains," *Economics and Business*, vol. 30, Apr. 2017. DOI: 10.1515/eb-2017-0010.

[12] SIA. "State of the satellite industry report." (2020), [Online]. Available: https://sia.org/news-resources/state-of-the-satellite-industry-report/ (visited on 02/05/2022).

[13] iDirect, "Overview of adaptive TDMA in an iDirect evolution network," Tech. Rep., Mar. 2020. [Online]. Available: https://www.idirect.net/wp-content/uploads/2020/03/TechBrief-AdaptiveTDMA.pdf (visited on 07/12/2021).

[14] ——, "Open training." (2021), [Online]. Available: https://www.idirect.net/products/training/ (visited on 11/26/2021).

[15] ——, "Satellite network calculator." (2021), [Online]. Available: https://www.idirect.net/products/satellite-network-calculator/ (visited on 11/26/2021).

[16] Gilat. "How-to tutorials." (2012), [Online]. Available: http://learn.gilat.com/course/index.php?categoryid=14 (visited on 11/26/2021).

[17] L. Luini, L. Emiliani, and C. Capsoni, "Planning of advanced satcom systems using ACM techniques: The impact of rain fade," in *Proceedings of the 5th European Conference on Antennas and Propagation (EUCAP)*, Apr. 2011, pp. 3965–3969.

[18] V. Pranjic, B. S. Mysore, N. Mazzali, and L. Emiliani, "Return link optimized resource allocation for satellite communications in the Ku/Ka-band," in *Proceedings on the 22nd Ka and Broadband Communications Conference and the 34th AIAA International Communications Satellite Systems Conference (ICSSC)*, Oct. 2016.

[19] C. Lacoste, N. Maturo, S. Chatzinotas, and L. Emiliani, "Optimization of the return link carrier planning for a constant coding and modulation satellite network," *Frontiers in Communications and Networks*, vol. 2, p. 52, Oct. 2021, ISSN: 2673-530X. DOI: 10.3389/frcmn.2021.744998. [Online]. Available: https://www.frontiersin.org/article/10.3389/frcmn.2021.744998.

[20] A. Petrolino, G. Codispoti, C. Riva, *et al.*, "Using the q/v-band aldo paraboni payload to validate future satellite systems: Test campaign and preliminary results of the qv-lift project," in *2018 2nd URSI Atlantic Radio Science Meeting (AT-RASC)*, 2018, pp. 1–3. DOI: 10.23919/URSI-AT-RASC.2018.8471633.

[21] C. Sacchi, T. Rossi, M. Murroni, and M. Ruggieri, "Extremely high frequency (EHF) bands for future broadcast satellite services: Opportunities and challenges," *IEEE Transactions on Broadcasting*, vol. 65, no. 3, pp. 609–626, Sep. 2019. DOI: 10.1109/TBC.2019.2892655.

[22] E. Cianca, T. Rossi, A. Yahalom, Y. Pinhasi, J. Farserotu, and C. Sacchi, "EHF for satellite communications: The new broadband frontier," *Proceedings of the IEEE*, vol. 99, no. 11, pp. 1858–1881, Nov. 2011. DOI: 10.1109/JPROC.2011.2158765.

[23] International Telecommunication Union (ITU). "Radiowave propagation." (2021), [Online]. Available: https://www.itu.int/rec/R-REC-P (visited on 07/13/2021).

[24] K. Paulson, L. Luini, N. Jeannin, B. Gremont, and R. Watson, "A review of channel simulators for heterogeneous microwave networks," *IEEE Antennas*

and Propagation Magazine, vol. 55, pp. 118–127, Oct. 2013. DOI: 10.1109/MAP.2013.6735480.

[25] L. Luini, "Modeling the space–time evolution of rain fields: Electromagnetic wave propagation applications," *IEEE Antennas and Propagation Magazine*, vol. 63, no. 4, pp. 12–20, Aug. 2021. DOI: 10.1109/MAP.2020.2976916.

[26] ITU, "Recommendation ITU-R P.1853-2: Time series synthesis of tropospheric impairments," Aug. 2019.

[27] N. Jeannin, L. Feral, H. Sauvageot, L. Castanet, and J. Lemorton, "Modeling of rain fields at large scale," in *2006 International Workshop on Satellite and Space Communications*, 2006, pp. 233–236. DOI: 10.1109/IWSSC.2006.256032.

[28] N. Jeannin, L. Féral, H. Sauvageot, L. Castanet, and F. Lacoste, "A large-scale space-time stochastic simulation tool of rain attenuation for the design and optimization of adaptive satellite communication systems operating between 10 and 50 GHz," *International Journal of Antennas and Propagation*, vol. 2012, May 2012. DOI: 10.1155/2012/749829.

[29] C. Capsoni, L. Castanet, P. Gabellini, *et al.*, "Use of space-time channel models and data for design and control of adaptive SatCom systems," in *Proceedings of the 5th European Conference on Antennas and Propagation, EUCAP 2011*, May 2011, pp. 3389–3392.

[30] C. Morel, P.-D. Arapoglou, M. Angelone, and A. Ginesi, "Link adaptation strategies for next generation satellite video broadcasting: A system approach," *IEEE Transactions on Broadcasting*, vol. 61, no. 4, pp. 603–614, Dec. 2015. DOI: 10.1109/TBC.2015.2470355.

[31] J. Arnau, D. Christopoulos, S. Chatzinotas, C. Mosquera, and B. Ottersten, "Performance of the multibeam satellite return link with correlated rain attenuation," *IEEE Transactions on Wireless Communications*, vol. 13, no. 11, pp. 6286–6299, Nov. 2014. DOI: 10.1109/TWC.2014.2329682.

[32] A. W. Marshall, *Inequalities: Theory of Majorization and Its Applications*, eng, Second Edition, ser. Springer Series in Statistics. 2011, ISBN: 9780387682761.

[33] O. Burdakov, C. Kanzow, and A. Schwartz, "Mathematical programs with cardinality constraints: Reformulation by complementarity-type conditions and a regularization method," *SIAM Journal on Optimization*, vol. 26, Oct. 2015. DOI: 10.1137/140978077.

[34] [Dataset] Center for International Earth Science Information Network - CIESIN - Columbia University, *Gridded population of the world, version 4 (GPWv4): Population density adjusted to match 2015 revision UN WPP country totals, revision 11*, NASA Socioeconomic Data and Applications Center (SEDAC), 2018. DOI: https://doi.org/10.7927/H4F47M65.

[35] L. Luini, "A comprehensive methodology to assess tropospheric fade affecting earth–space communication systems," *IEEE Transactions on Antennas and Propagation*, vol. 65, no. 7, pp. 3654–3663, Jul. 2017. DOI: 10.1109/TAP.2017.2700883.

[36] ITU, "Recommendation ITU-R P.618-13: Propagation data and prediction methods required for the design of earth-space telecommunication systems," Dec. 2017.

[37] Ofcom. "Delivering the broadband universal service." (Jun. 2019), [Online]. Available: https://www.ofcom.org.uk/__data/assets/pdf_file/0019/151354/statement-delivering-the-broadband-universal-service.pdf.

[38] ETSI, "Second generation DVB interactive satellite system part 2: Lower layers for satellite standard," Tech. Rep. ETSI standard EN 301 545-2, 2014. [Online]. Available: https://www.etsi.org/.

[39] A. Kyrgiazos, B. Evans, P. Thompson, P. T. Mathiopoulos, and S. Papaharalabos, "A terabit/second satellite system for european broadband access – a feasibility study," *International Journal of Satellite Communications and Networking*, vol. 32, Mar. 2014. DOI: 10.1002/sat.1067.

[40] MathWorks. "Optimization toolbox." (2021), [Online]. Available: https://nl.mathworks.com/products/optimization.html (visited on 09/01/2021).

[41] S. J. Maher, T. Fischer, T. Gally, *et al.*, "The SCIP Optimization Suite 4.0," Zuse Institute Berlin, ZIB-Report 17-12, Mar. 2017. [Online]. Available: http://nbn-resolving.de/urn:nbn:de:0297-zib-62170.

[42] M. Grant and S. Boyd, *CVX: Matlab software for disciplined convex programming, version 2.1*, Mar. 2014. [Online]. Available: http://cvxr.com/cvx (visited on 11/11/2021).

Clement Lacoste was born in Cagnes-sur-mer, France, in 1995. He received the M.Sc. degree in Telecommunications and Networks from the Ecole Nationale Supérieure d'Electrotechnique, d'Electronique, d'Informatique, d'Hydrolique et des Télécommunications (ENSEEIHT), Toulouse, in 2019. He is currently working toward the Ph.D. degree as a Doctoral Researcher at the Interdisciplinary Centre for Security, Reliability, and Trust (SnT) of the University of Luxembourg. His research interests include satellite network sizing, optimization of resource allocation, and tropospheric attenuation modelling.

Wallace A. Martins (S'07–M'12–SM'20) received the electronics engineer degree, and the M.Sc. and D.Sc. degrees in electrical engineering from the Federal University of Rio de Janeiro (UFRJ), Rio de Janeiro, Brazil, in 2007, 2009, and 2011, respectively. He was a Research Visitor at the University of Notre Dame, USA, in 2008, Université de Lille 1, France, in 2016, and Universidad de Alcalá, Spain, in 2018. He was an Associate Professor at the Department of Electronics and Computer Engineering (DEL/Poli) and the Electrical Engineering Program (PEE/COPPE), UFRJ, from 2013 to 2022. He was Academic Coordinator and Deputy Department Chairman (DEL/Poli), UFRJ, from 2016 to 2017. He is currently a Research Scientist working with the Interdisciplinary Centre for Security, Reliability and Trust (SnT), University of Luxembourg. His research interests include digital signal processing and telecommunications, with focus on equalization and beamforming/precoding for terrestrial and non-terrestrial (satellite) wireless communications. He is a member (Associate Editor) of the Editorial Boards of the IEEE SIGNAL PROCESSING LETTERS and the EURASIP Journal on Advances in Signal Processing. He was the recipient of the Best Student Paper Award from EURASIP at EUSIPCO-2009, Glasgow, Scotland, the 2011 Best Brazilian D.Sc. Dissertation Award from Capes, and the Best Paper Award at SBrT-2020, Florianópolis, Brazil.

Symeon Chatzinotas (S'06–M'09–SM'13) is currently Full Professor / Chief Scientist I and Head of the SIGCOM Research Group at SnT, University of Luxembourg. In the past, he has been a Visiting Professor at the University of Parma, Italy and he was involved in numerous Research and Development projects for the National Center for Scientific Research Demokritos, the Center of Research and Technology Hellas and the Center of Communication Systems Research, University of Surrey. He received the M.Eng. degree in telecommunications from the Aristotle University of Thessaloniki, Thessaloniki, Greece, in 2003, and the M.Sc. and Ph.D. degrees in electronic engineering from the University of Surrey, Surrey, U.K., in 2006 and 2009, respectively.

He was a co-recipient of the 2014 IEEE Distinguished Contributions to Satellite Communications Award, the CROWNCOM 2015 Best Paper Award and the 2018 EURASIC JWCN Best Paper Award. He has (co-)authored more than 400 technical papers in refereed international journals, conferences and scientific books. He is currently in the editorial board of the IEEE Open Journal of Vehicular Technology and the International Journal of Satellite Communications and Networking.

Luis D. Emiliani (M'04-SM'21) received the titles of B.E.E and M.Eng from Universidad Pontificia Bolivariana, Medellin, CO. in 1999 and 2003. At present he is with SES, in the spectrum development group, responsible for identifying new spectrum opportunities and set spectrum policy for both GSO and NGSO systems. His main interests are in the application of propagation techniques to solve practical sharing and communications scenarios. Mr. Emiliani is a Chartered Engineer with the UK Engineering council, and member of the Institution of Engineering and Technology.